Modelling of collective Thomson scattering from collisional plasmas

2003 J. Phys. A: Math. Gen. 36 5981

(http://iopscience.iop.org/0305-4470/36/22/320)

INSTITUTE OF PHYSICS PUBLISHING JOURNAL OF PHYSICS A: MATHEMATICAL AND GENERAL

J. Phys. A: Math. Gen. **36** (2003) 5981–5989 PII: S0305-4470(03)55359-8

Modelling of collective Thomson scattering from collisional plasmas

T E Tierney IV, D S Montgomery, J F Benage Jr, F J Wysocki and M S Murillo

Los Alamos National Laboratory, PO Box 1663, Mailstop E526, Los Alamos, NM 87545, USA

Received 29 October 2002, in final form 19 February 2003
Published 22 May 2003
Online at stacks.iop.org/JPhysA/36/5981

Abstract

Anomalous broadening of ion-acoustic modes has been observed using collective Thomson scattering from both the electron plasma and ion-acoustic waves in ion-collisional plasmas. Ion-acoustic waves may be broadened by Landau damping, plasma inhomogeneities and instrumental effects. A model was constructed to calculate the contribution of these effects based upon spatially and spectrally resolved measurements of collective Thomson scattering. Collisional broadening effects were then calculated using a modification of the Mermin formalism. The computational model was used to interpret experimental measurements of collisional damping rates in dense, moderately coupled, plasmas. Collisional broadening is weakly dependent of ion-acoustic frequency in nearly isothermal plasmas; and therefore collective Thomson scattering can be used as a measurement technique for collisional damping rates provided all additional broadening mechanisms are taken into account. This paper further demonstrates that modelling of collective Thomson scattering from ion-collisional ion-acoustic modes must account for inhomogeneities, Landau damping, and collisions in order to evaluate plasma parameters, such as temperature and average ionization.

PACS numbers: 07.60.−j, 52.20.Hv, 52.25.−b, 52.25.Mq, 52.25.Gj

1. Introduction

The presence of ion–ion collisions has been predicted to broaden the ion-acoustic wave (IAW) and reduce the effective acoustic speed through collisional damping [1–3]. Such effects can be measured using collective Thomson scattering (CTS) from IAWs. The spectral separation of the IAW CTS resonances is used as a temperature diagnostic for many experiments; however, the influences of ion–ion collisions and inhomogeneities can introduce large uncertainties in these measurements. Until now, the broadened IAW CTS has not been used as a collisional damping rate diagnostic, primarily due to the features' sensitivity to plasma inhomogeneities.

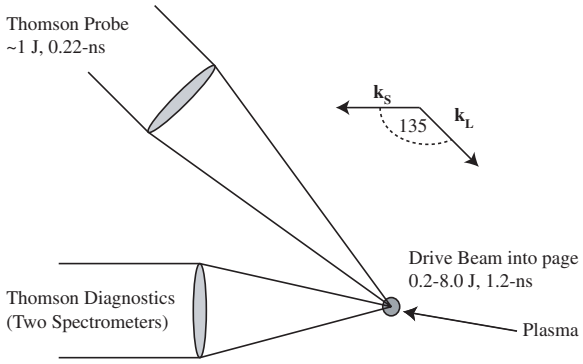

Figure 1. Schematic of the experimental arrangement for collective Thomson scattering measurements at an angle of 135°, and the plasma is expanding out of the page.

This is unfortunate, since the damping of IAWs plays a critical role in the growth of stimulated Brillouin scattering, an area of serious concern for the National Ignition Facility [4].

An experiment was conducted on the Los Alamos National Laboratory Trident Laser Facility [5] to study the effects of ion–ion collisions in dense plasmas. The conditions and composition of the plasma were selected such that electron–ion collisions are weak, and thus, the experiment focuses on the effects due to ion–ion collisions alone. A Joule-level frequency-doubled (527 nm), 1.2 ns, square drive pulse produced a $n_e \sim 10^{20}$ cm^{-3}, $T_e \sim$ 100 eV plasma from solid aluminium, parylene (CH) or polyethylene (CH_2) targets. Afterwards, a Joule-level, frequency-tripled (351 nm), 0.2 ns pulse interacted with the plasma to produce CTS from IAWs and electron-plasma waves (EPWs), see figure 1.

Two 0.5 m imaging spectrometers were fielded at a scattering angle of 135° to record the CTS from IAWs and EPWs. The first spectrometer resolved the scattering from IAWs using a high dispersion grating, while a low dispersion grating was used in the second system to simultaneously resolve scattering from EPWs. Both spectrometers were fielded along the same optical path to provide spatially correlated images that are spectrally and spatially resolved. Images were taken both parallel (radial) and perpendicular (axial) to the target in order to characterize the plasma. Axial images were used to characterize the axial gradients of temperature and density, while the radial images were used for the broadening measurements.

The scattering spectrum from the EPWs was used to obtain the peak densities as a function of radius. Radial velocity and temperature profiles were inferred from the position and separation of the IAW peaks respectively. The radial velocity profile was found from the data using a fourth-, fifth- or sixth-order polynomial fit to the observed Doppler shifts of the centroid positions of both peaks. The magnitude of the velocity is estimated using the centre position between the peaks from the equation $v = c\delta\lambda/\lambda_0$. As will be shown in section 3, the interpretation of what temperature corresponds to in terms of the separation is dependent upon both the amount of collisional damping and the characteristics of the plasma inhomogeneities.

The experiment measured half-widths at half-maximum (HWHM) of CTS ion-acoustic resonances of the order of the ion-acoustic frequency. A significant fraction of this broadening was due to the temperature, density and velocity profile of the plasma. Landau damping and the optical elements of the diagnostics also contributed to the broadening of the scattering features.

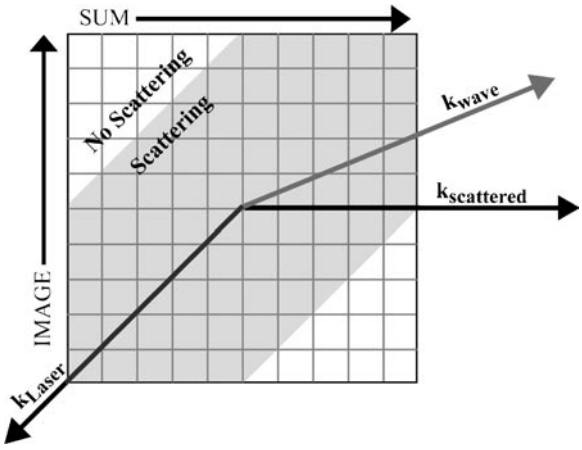

Figure 2. A two-dimensional grid was created for the simulation, where each grid point is given a specific plasma parameter. This spectrum is spatially integrated along the line-of-sight of the diagnostics to account for inhomogeneity broadening.

The model described below was developed to quantify the broadening contributions of the inhomogeneities, instruments and both Landau and collisional damping mechanisms. Collisions are included by a simple Mermin correction to the scattering form factor. Although several other models exist, this model conserves charge unlike the more general BGK [6] treatment and has runtimes of less than an hour unlike the Fokker–Planck-based methods [2, 7]. The results of the comparison to experiment are discussed elsewhere [8].

2. The model

The model starts with a 2D grid, shown in figure 2, where each grid point is assigned a specific n_e, Z, T_e, T_i and $\mathbf{v}$. Independent ion and electron temperatures can be used; however, the short thermal equilibration times for the experimental plasmas should place T_i close to T_e. A calculation of the scattering form factor, $S_{ee}(\mathbf{k}, \omega)$, is performed for each cell individually. The routine then calculates the spectrum scattered by both IAWs and EPWs from the individual grid points. The cylindrically symmetric temperature, density and velocity profiles are integrated along the line-of-sight to account for plasma inhomogeneities. A simulated laser probe produces scattering with only those gridpoints that would be interacted with by the real experimental probe, shown as the shaded region in figure 2. Dawson–Oberman [9] inverse Bremsstrahlung absorption is used to attenuate the probe and the scattered light. Although the model can calculate scattering from any CTS angle, the experimental angle of 135° was used. A spectral limitation of three-pixel instrument resolution is taken into account by folding in a Gaussian blurring function into the calculated spectrum.

The frequency shift of the low frequency IAW peaks relative to the laser frequency (which may be Doppler shifted) is dominated by the electron temperature,

$$\omega_{\mathrm{iaw}} \cong k_{\mathrm{iaw}} \sqrt{\frac{T_e}{M}\left(\frac{\bar{Z}}{1 + k_{\mathrm{iaw}}^2 \lambda_D^2}\right) + \gamma_i \frac{T_i}{M}} \tag{1}$$

where $\mathbf{k}_{\mathrm{iaw}} = \mathbf{k}_{\mathrm{Laser}} - \mathbf{k}_s$. The temperature, in combination with the ion density profile, is used to calculate the ionization using either Thomas–Fermi [10], Saha–Boltzman or time-dependent, detailed atomic structure collisional-radiative models [11].

A radially expanding velocity field is created for the grid with a radially dependent amplitude profile. The axial velocity due to the plasma's expansion from the target is ignored since $\mathbf{k}_s \cdot \mathbf{v} = 0$. The radially varying velocity profile broadens the IAW spectrum when the scattering is integrated in the direction of the detector. The radially symmetric velocity vector field is incorporated into the model through the frequency relation, $\Delta\omega = \omega_s - \omega_0 - \mathbf{k}_s \cdot \mathbf{v}$, prior to calculating the scattering intensity.

The maximum density was estimated from the data using the maximum frequency shift of the EPW peak and the Bohm–Gross relation,

$$n_e = 1.77 \times 10^{-5} \left(\frac{\omega_{epw}^2}{1 + 3k_{epw}^2 \frac{T_e}{m_e}} \right) \tag{2}$$

with ω_{epw} as the EPW frequency, the electron mass and temperature, m_e and T_e respectively, and k_{epw} is found by $\mathbf{k}_{epw} = \mathbf{k}_{Laser} - \mathbf{k}_s$. Independent isotropic Maxwellian distribution functions are found and are normalized to the thermal velocity for each species. The ions are treated as individual species for each element present and for the different charge state ions of the same element. The susceptibility is then calculated using

$$\chi_j = \frac{-\alpha_j^2}{2} \zeta' \left(\frac{\Omega_j \alpha_j}{\sqrt{2}} \right) = \frac{\beta_j Z_j^2 T_e}{2\bar{Z} T_i \left(k\lambda_{Dj} \right)^2} \zeta' \left(\frac{\Omega_j \alpha_j}{\sqrt{2}} \right) \tag{3}$$

where $\bar{Z}$ is the average ionization, Ω_j is the frequency space normalized to the plasma frequency, Z_j is the charge of the species, λ_{Dj} is the Debye length, β_j is the fractional content and α_j is the scattering parameter for each species, $\alpha_j = 1/k\lambda_{Dj}$ of species j. ζ' is the plasma dispersion function represented as a derivative of the Fried–Conte Z-function [12].

The effect of collisional damping is included through the addition of a complex computational constant into the argument of the susceptibilities in the particle conserving Mermin form [13]. The susceptibilities of the ions and electrons are calculated independently of one another. The damping frequency for each species, ν_e or ν_i, is defined in terms of the electron plasma frequency, $\nu = \gamma_{ia}/\omega_{pe}$, to include a density dependence. Since the ion–ion collisions are of interest here, only the ion collision frequency is considered in this discussion. Each susceptibility could be modified with separate collision frequencies using $z = \Omega + i\nu$. This substitution is used in the Mermin form of the susceptibilities for each species [13],

$$\chi_\nu(k, \Omega) = \frac{\left(1 - \frac{i\Omega}{\nu}\right) \chi(k, z) \chi(k, 0)}{\chi(k, z) - \frac{i\Omega}{\nu} \chi(k, 0)}. \tag{4}$$

This is then used in calculating the plasma dielectric function, $\varepsilon = 1 + \sum_j \chi_j = 0$, and the scattering form factor is calculated using the case of multiple ion species [14, 15],

$$S_{ee}(k, \omega) = \frac{2\pi}{k} \left(f_e \left(\frac{\omega}{k} \right) \left| \frac{1 - \chi_e \, \mathrm{Im}(\varepsilon)}{|\varepsilon|^2} \right| + \sum_n \beta_n Z_n^2 f_{i,n} \left(\frac{\omega}{k} \right) \left| \frac{\chi_e \, \mathrm{Im}(\varepsilon)}{|\varepsilon|^2} \right| \right) \tag{5}$$

where $\mathrm{Im}(\varepsilon)$ is the imaginary part of the dielectric function.

Assuming an incident laser power, P_I, the power scattered at grid point x, y into solid angle $d\Omega$ at a distance R is found by [16]

$$P_{x,y}(R, \omega) = P_I r_0^2 L \frac{d\Omega \, d\omega_s}{2\pi} |\hat{s} \times (\hat{s} \times \hat{E}_{I0})|^2 n_e \, S(k, \omega) \tag{6}$$

where L is the length of the interaction region within the plasma and r_0 is the classical electron radius. The total scattered power is calculated by summing the power radiated from each grid point in the direction of the diagnostics and performing a sum over the range of scattering angles to account for the acceptance angle of the optics.

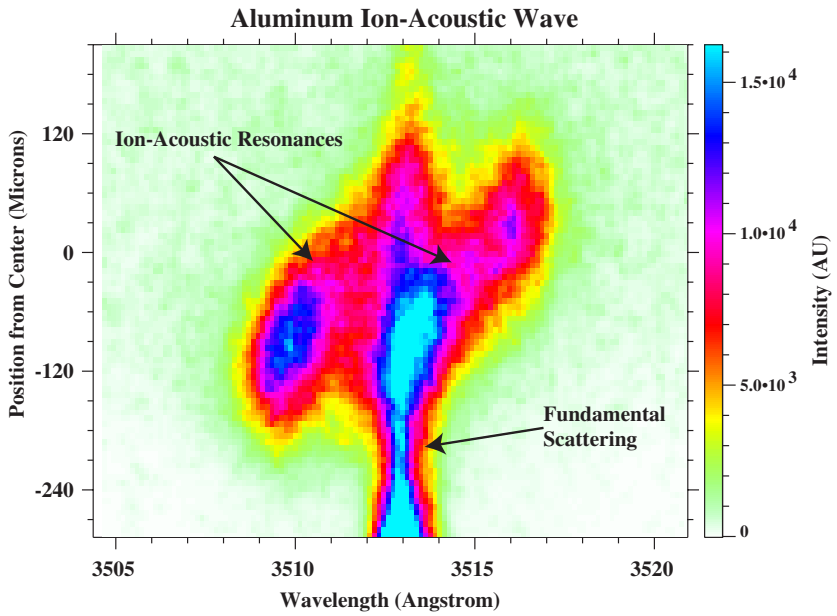

Figure 3. Collective Thomson scattering from ion-acoustic waves spectrum, where the two slanted peaks are the velocity-Doppler shifted ion-acoustic resonances. Some fundamental scattering from the plasma's critical surface is visible at 3513 Å.

The model outputs spatially and spectrally resolved images of scattering from IAWs and EPWs. The simulated IAW scattering images are then fit using only two Gaussians with the same fitting routine used to analyse the experimental data. The fundamental is not produced in the simulated data. The widths and centroid positions of the peaks, as well as the centre position between the peaks, are compared to the experimental profiles of the EPW and IAW scattering spectra. The model was verified against known analytic results and collisionless plasma experiments prior to calculating collisional effects.

The IAW spectrum is extremely sensitive to shape, direction and amplitude of the velocity as well as the temperature, but weakly sensitive to the density profile. The velocity profile, as measured by the peak positions, was required to reproduce the centroids of the experimental IAW spectrum over the whole spatial extent of the image. As an additional check the position of zero frequency as defined by the simulated central position between the peaks was compared to a similar measurement in the experimental data. As a result, the model produces an experimentally verifiable broadening due to the inhomogeneity, Landau damping and instrumental effects, in addition to the collisionally broadened spectrum.

3. Discussion

Figure 3 shows a 1D radial image taken at 150 μm from the target surface. The IAWs scattering spectrum is spectrally resolved, and each spatial position of this image includes an integral over the line-of-sight spatial profile. This experimental data is fit with three Gaussians to remove stray light from the fundamental at 3513 Å. Stray light interferes with some regions of the broadening measurement when it happens to fall directly on top of one of the scattering peaks. Figure 4 shows the simulated HWHM broadening for three sets of

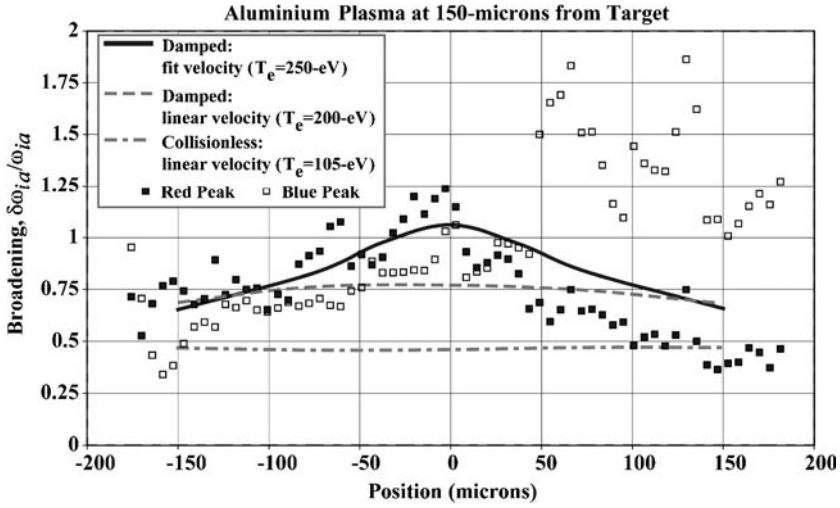

Figure 4. The collisionless inhomogeneous model produces less than half of the measured broadening. Collisions, included using the Mermin form, are able to account for the shape and amplitude of the broadening, but a dramatic temperature increase was required to hold the resonance positions constant. Stray light interferes with the width fits for the blue peak in the region 50–200 μm.

conditions compared to the experimental data. The solid and open boxes are the average HWHM broadening measurements of the red and blue peaks from an aluminium plasma experiment. The blue half-widths jump up to twice the normal half-widths in the region where the stray light falls on top of the peak. In those regions, the fitting routine is unable to discern between the stray light and the obscured peak, and therefore, the width measurement from that peak has a high uncertainty. The unobscured peak, in this case the red peak, gives a clean broadening measurement with little uncertainty.

When the inhomogeneous, collisionless model results are compared to the experimental data, the inhomogeneity, Landau damping and instrumental effects account for HWHM broadening of nearly half of the ion-acoustic frequency in this moderately collisional regime, as shown by the dash-dot line in figure 4. The dashed curve was produced using a linearly increasing radial velocity profile in the collisional model with all additional broadening effects including a damping frequency, $\nu_{\mathrm{i}} = 0.0035\omega_{\mathrm{pe}}$. And finally, the solid curve corresponds to the HWHM broadening produced by the simulation with the same damping frequency where the radial velocity profile was taken from the Doppler shift observed in the IAW data.

This inhomogeneous damping model creates a large frequency *downshift* towards zero frequency with increasing collisional damping frequency. As a test case, we considered an isothermal homogeneous plasma, where there is zero flow and uniform density, the model produces a 10–15% frequency downshift for $\nu_{\mathrm{i}} = 0.002$–$0.004\omega_{\mathrm{pe}}$, shown in figure 5. The solid curve shows a rapid shift (left ordinate) of the resonance towards zero frequency as the damping frequency is increased. This homogeneous result agrees with the results of other homogeneous models presented in literature [7, 17, 18]. Some of the frequency downshift may be the result of a decrease in the ratio of specific heats for the ions from 3 to 5/3, while the ratio of specific heats for the electrons remains at 1. With the assumption that $T_{\mathrm{e}} = T_{\mathrm{i}}$, the dashed curve shows how much one would have to increase the inferred temperature (right ordinate) in order to hold the frequency position constant. Since broadening increases

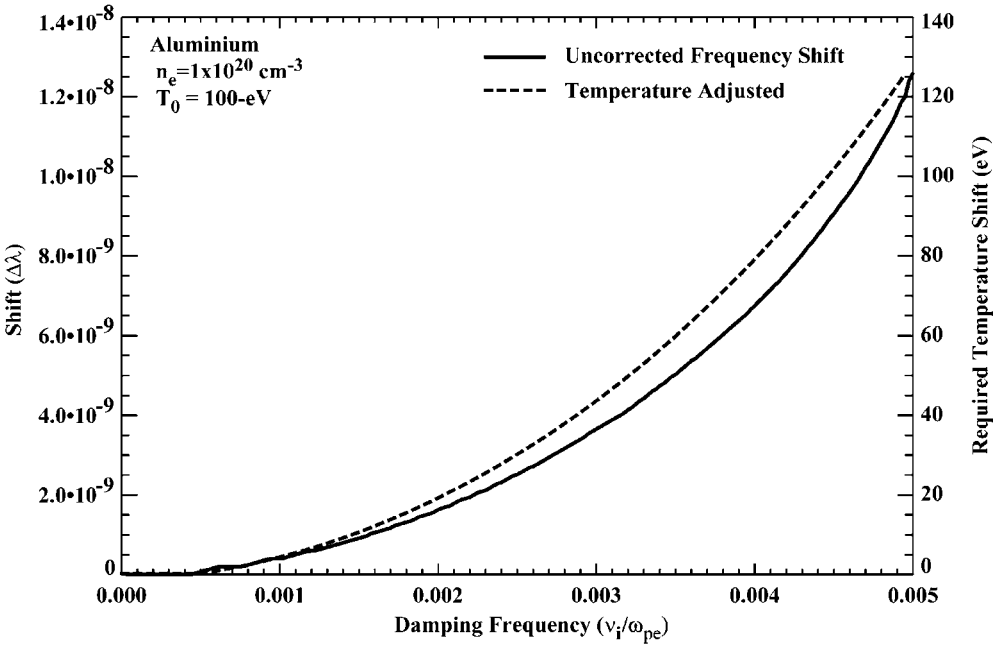

Figure 5. The frequency downshift, or frequency shift towards zero frequency, of an ion-acoustic scattering resonance as a function of applied damping for a homogeneous plasma. Zero shift corresponds to where the centroid position of the ion-acoustic scattering resonance corresponds to the collisionless value. Relative to the collisionless model a higher temperature was required in order to fit the experimental data.

with damping in this regime, the temperature was used as a computational knob to hold the resonance frequency constant.

A frequency shift presents a problem when one intends to use CTS from IAWs as a temperature diagnostic for collisional, inhomogeneous plasmas. For example, we found that the collisionless model required a temperature of 100 eV to match the spectral separations of the IAWs for an aluminium shot; whereas, the modelled temperature had to be increased to 250 eV when collision frequencies of $\nu_{\mathrm{i}} = 0.0035\omega_{\mathrm{pe}}$ were included. This high collisional damping frequency is approximately equal to the ion-acoustic frequency. The required temperature increase, $\Delta T_{\mathrm{e}} \sim 145$ eV, is over twice the 60 eV value predicted by the homogeneous model. We observed that the presence of inhomogeneities amplifies the frequency downshift, and thus, the inferred temperature is much higher than what one would expect from a homogeneous model.

The magnitude of the collisional damping frequency is calculated as constant relative to the electron plasma frequency, whereas a more appropriate treatment would scale the damping rate as linear with density. Our experimental measurements indicated that the separation of the peaks was independent of position to be within the statistical noise of the measurements; therefore, it is reasonable to neglect the temperature dependence of the collision frequency in this case. While the higher density material will scatter more light, the effects of damping have the potential to reduce this amplitude below that of the lower density material. The lower density material has a higher radial velocity field associated with it than the high density material in the model, so the peak amplitude is asymmetrically drawn towards zero

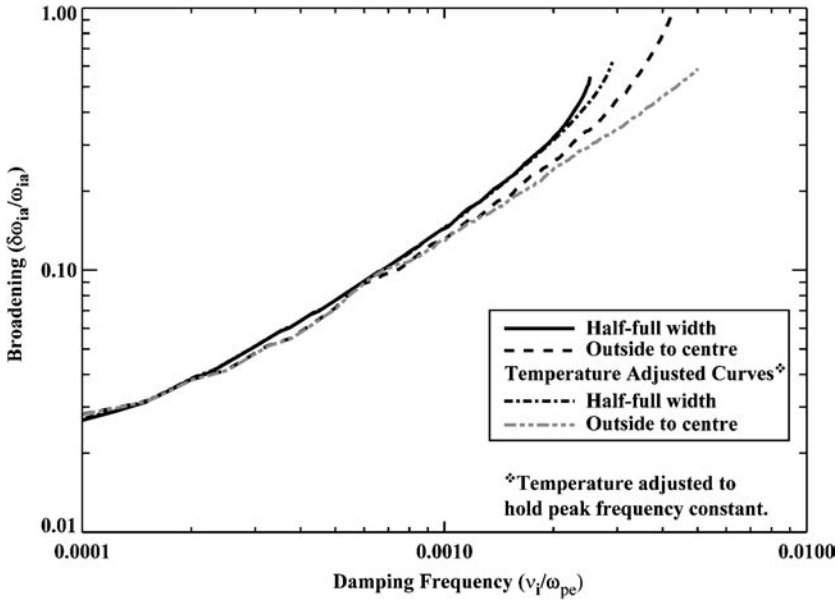

Figure 6. A comparison of the temperature fixed and the temperature adjusted broadening produced by the model shows that the broadening is relatively independent of the centroid positions of the IAW resonance.

frequency. Therefore, when inhomogeneities are included in the damped plasma model, the simulated frequency separation is smaller than that produced in the homogeneous case.

The dependence of the IAW CTS spectral widths upon the applied collisional damping frequency is shown in figure 6. The solid and dashed curves correspond to the half-widths measured by half the full width and from the outside of one peak at half amplitude to the centre of that peak respectively for the homogeneous case at $T_e = 100$ eV. The dash-dot and dash-dot-dot curves represent similar measurements where the temperature has been adjusted to hold the frequency position of the peak constant. An interesting observation is that the level of broadening is independent of resonance position until damping frequencies of $0.002\omega_{pe}$. This appears to indicate that this model provides estimates of collisional damping rates with reasonable accuracy despite the temperature uncertainty.

For the purpose of interpreting our experimental results, we used the collisionless model to estimate the plasma temperature, while at the same time used the Mermin form to estimate the damping and collision rates. It is clear that a more accurate treatment must be developed in order to identify the electron temperature. This treatment might use known collision frequencies to calculate the collisional damping rates.

4. Conclusions

We have created a simple, collisional CTS model that can be used to compare to experimental IAW broadening data for ion–ion collisional damping rate measurements in inhomogeneous plasmas. In this model, the results demonstrated that collisional broadening is independent of CTS IAW resonance position for nearly isothermal plasmas. Once instrument, inhomogeneity

and Landau damping mechanisms are taken into account, this broadening technique may be used as a collisional damping rate measurement technique.

The model further revealed that the effect of a moderate frequency downshift, produced by ion–ion collisional damping, is amplified by plasma inhomogeneities such as velocity or density profiles. For the conditions considered here, the frequency downshift was more than doubled. This demonstrates that more experimental and theoretical development is required before resonance positions can be used for determining temperatures and average ionization in inhomogeneous, ion–ion collisional plasmas.

Acknowledgments

We wish to acknowledge Dr J Abdallah at Los Alamos National Laboratory for providing time-dependent collisional-radiative equilibrium calculations of ionization balances for aluminium and carbon. We thank Dr S Glenzer of Lawrence Livermore National Laboratory and Professor W Rozmus of the University of Alberta for their suggestions on the analysis of the experimental data. We also wish to acknowledge the valuable input provided by Professor N Rostoker and Professor L Chen of University of California, Irvine. This work was performed under the auspices of the US Department of Energy by the Los Alamos National Laboratory under contract no W-7405-ENG-36.

References

[1] Myatt J F *et al* 1998 *Phys. Rev.* E **57** 3383
[2] Zheng J, Yu C X and Zheng Z J 1999 *Phys. Plasmas* **6** 435
[3] Tracy M D *et al* 1993 *Phys. Fluids* B **5** 1430
[4] MacGowan B J *et al* 1996 *Phys. Plasmas* **3** 2029
[5] Moncur N K *et al* 1995 *Appl. Opt.* **34** 4274
[6] Bhatnagar P L, Gross E P and Krook M 1954 *Phys. Rev.* **94** 511
[7] Linnebur E J and Duderstadt J J 1973 *Phys. Fluids* **16** 665
[8] Tierney T E *et al* 2002 Collective Thomson Scattering measurements of ion-acoustic wave broadening in moderately coupled, moderately collisional plasmas *PhD Thesis* University of California, Irvine (unpublished)
[9] Dawson J M and Oberman C 1962 *Phys. Fluids* **5** 517
[10] More R 1981 UCRL-84991
[11] Abdallah J 2002 Private communication
[12] Fried B D and Conte S D 1961 *The Plasma Dispersion Function* (New York: Academic)
[13] Mermin N D 1970 *Phys. Rev.* B **1** 2362
[14] Evans D E 1970 *Plasma Phys.* **12** 573
[15] Evans D E and Katzenstein J 1969 *Rep. Prog. Phys.* **32** 207
[16] Sheffield J 1975 *Plasma Scattering of Electromagnetic Radiation* (New York: Academic)
[17] Ono M and Kulsrud R M 1975 *Phys. Fluids* **18** 1287
[18] Mostovych A N and DeSilva A W 1986 *Phys. Rev.* A **34** 3238